Measurements and simulations of focused beam for orthovoltage therapy

Hassan Abbas[a)]
Department of Therapeutic Radiology, Yale University School of Medicine, Yale-New Haven Hospital, New Haven, 344 Lane Street Hamden, Connecticut 06514

Dip N. Mahato[b)]
Intel Corporation, Mail-Stop RA3-410, 2501 NW 229th Avenue, Hillsboro, Oregon 97124

Jahangir Satti[c)]
Department of Radiation Oncology, Albany Medical Center, 43 New Scotland Avenue, Albany, New York 12208

C. A. MacDonald[d)]
Department of Physics, University at Albany, SUNY, 1400 Washington Avenue, Albany, New York 12222

(Received 3 July 2013; revised 31 January 2014; accepted for publication 7 February 2014; published 7 March 2014)

Purpose: Megavoltage photon beams are typically used for therapy because of their skin-sparing effect. However, a focused low-energy x-ray beam would also be skin sparing, and would have a higher dose concentration at the focal spot. Such a beam can be produced with polycapillary optics. MCNP5 was used to model dose profiles for a scanned focused beam, using measured beam parameters. The potential of low energy focused x-ray beams for radiation therapy was assessed.
Methods: A polycapillary optic was used to focus the x-ray beam from a tungsten source. The optic was characterized and measurements were performed at 50 kV. PMMA blocks of varying thicknesses were placed between optic and the focal spot to observe any variation in the focusing of the beam after passing through the tissue-equivalent material. The measured energy spectrum was used to model the focused beam in MCNP5. A source card (SDEF) in MCNP5 was used to simulate the converging x-ray beam. Dose calculations were performed inside a breast tissue phantom.
Results: The measured focal spot size for the polycapillary optic was 0.2 mm with a depth of field of 5 mm. The measured focal spot remained unchanged through 40 mm of phantom thickness. The calculated depth dose curve inside the breast tissue showed a dose peak several centimeters below the skin with a sharp dose fall off around the focus. The percent dose falls below 10% within 5 mm of the focus. It was shown that rotating the optic during scanning would preserve the skin-sparing effect of the focused beam.
Conclusions: Low energy focused x-ray beams could be used to irradiate tumors inside soft tissue within 5 cm of the surface. [http://dx.doi.org/10.1118/1.4866224]

Key words: polycapillary optics, focused x-ray beam, focus spot, skin sparing, MCNP

1. INTRODUCTION

One of the limiting factors in early external beam radiation therapy was skin dose. Low energy x rays deposit the maximum dose at the surface. In order to reduce the skin dose when treating the deep seated tumors, megavoltage beams were developed. Instead, focusing a low energy x-ray beam could result in spreading the beam across the skin surface while increasing the beam intensity at the tumor. Such a beam can be produced with polycapillary optics. Polycapillary focusing and collimating lenses were invented in the 1980s.[1] They contain arrays of hundreds of thousands of hollow capillary tubes fused together, as shown in Fig. 1.

X rays can be transmitted down a curved hollow tube as long as the tube is small enough, and bent gently enough, to keep the angles of incidence less than the critical angle for total reflection, θ_c, as shown in Fig. 2. The critical angle for borosilicate glass is approximately

$$\theta_c = \frac{30\,\text{keV}}{E}\text{mrad}, \tag{1}$$

which is approximately 1.7° for 1 keV photons and 0.086° for 20 keV photons.

The requirement that the incident angles remain less than the critical angle necessitates the use of tiny tubes. However, mechanical limitations prohibit the manufacture of capillary fibers with outer diameters smaller than about 300 μm. For this reason, polycapillary fibers, which have tube diameters that are much smaller than the fiber diameter, are employed. Most commercial optics are one-piece, monolithic, optics, as sketched in Fig. 3.[2] Polycapillary optics are used in diverse applications, especially for materials analysis such as x-ray diffraction,[3,4] fluorescence, and spectroscopy[5] and have been investigated for a number of medical applications.[6–9] A focusing polycapillary optic was used in our study to obtain a focused x-ray beam. Polycapillary optics are a good match for therapy applications as they have been shown to be robust

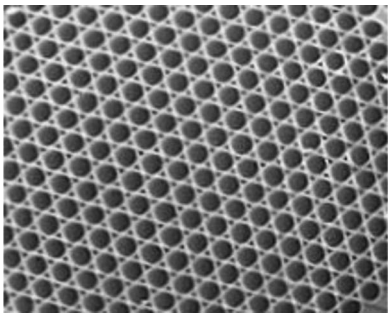

FIG. 1. Cross sectional view of polycapillary lens, with 50 μm diameter channels. The channels in the device used in this work were approximately 6 μm.

with respect to radiation damage, exhibiting no change in performance after being subjected to 1 MJ/cm^2 on the optic face in synchrotron studies. That test corresponded to input radiation that would be sufficient to treat thousands of patients at 10–80 Gy total tumor dose.[10]

The potential of low-energy focused x-ray beams for radiation therapy was assessed. The schematic diagram of the proposed method is shown in Fig. 4. MCNP5 (Ref. 11) was used to model a low-energy focused x-ray beam, using measured beam parameters. Dose calculations were performed inside a breast tissue phantom.

One of the potential applications of the proposed method could be accelerated partial breast irradiation (APIB). The standard treatment method for early stage breast cancers is breast-conserving surgery (lumpectomy) followed by the radiation therapy. In order to reduce the treatment time, APIB can be used instead of the conventional radiation therapy. APIB delivers radiation to the area immediately around the lumpectomy site instead of treating the entire breast. Intracavitary brachytherapy[12,13] (MammoSite) and electronic brachytherapy[14] are two radiation treatment options used in the majority of accelerated partial breast irradiation cases along with permanent seed implants and HDR. Both of these methods are invasive. The proposed method is noninvasive and can give high conformal dose to the target while sparing the skin. Focused orthovoltage beams have also been proposed for glioblastomas.[15] For that study, a curved monochromatic crystal was used as the focusing device. This device produces a much longer depth of field, almost a line focus, compared to a more spot-like focus from the polycapillary optic used in this study. The monochromatic beam from the

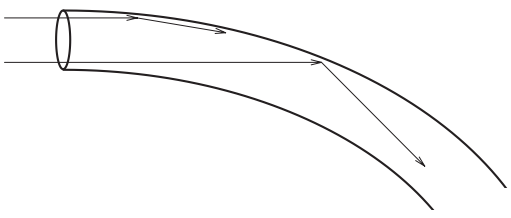

FIG. 2. X rays traveling in a bent capillary tube. The trajectory of the ray entering at the top at grazing incidence is projected onto the page, but in three dimensions will "toboggan" in a constant radius spiral. The x ray entering at the bottom (closest to the center of curvature) strikes at a larger angle.

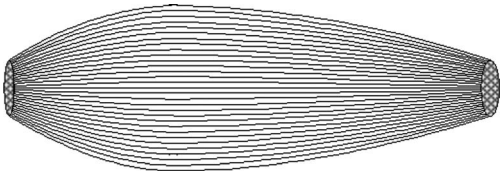

FIG. 3. Sketch of the interior channels of a monolithic polycapillary optic. Monolithic optics can be focusing or collimating.

curved crystal reduces the effects of beam hardening, but at the cost of lowered intensity compared to simple filtered white beam radiation focused with a polycapillary optic.

2. MATERIAL AND METHOD

2.A. Measurements

Measurements were made with a polycapillary lens (X-ray Optical Systems, Inc., serial number 4280) used to collect x rays from a conventional divergent x-ray source and redirect them to make a focused x-ray beam.[16] The measurements were performed on a tungsten anode microfocus source at 50 kV at 0.05 mA, 2.5 W. Since measurements were performed with a very low power source, an EG&G Ortec high-purity germanium (HPGe) detector was used to measure the single photon count rates. The detector allowed measurement of the x-ray spectrum of the beam from the optic. Lead shielding was used at the entrance and exit of the optic casing and in the surrounding area of the optic to prevent the leakage to decrease the background to less than 1%. An aluminum filter of 0.78 mm thickness was used to reduce the detector dead time to less than 10%. The optic was mounted on a stage fitted with actuators to move in three dimensions. The actuators were run through a Newport programmable motional controller model PMC 200-P by software [automatic control program (ACP)]. The lens was moved in the x and y direction until the maximum count rate was obtained. The lens was then scanned in both the x and the y directions using the "scan" mode of the ACP software. The software records the counts as a function of the position of the lens. After each scan the lens was moved, so the lens was located at the maximum of the counts-versus-lens-position curve. This was iterated for alternating directions, until the location of the maximum counts was unchanged. Once the lens was characterized and aligned with the x-ray beam, the size and position of focal point was determined. The position of the focal point was determined

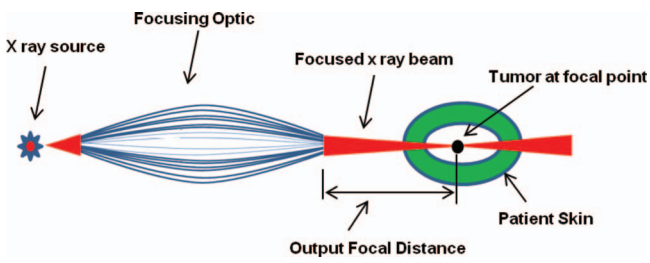

FIG. 4. Schematic diagram of a focused x-ray beam using polycapillary optics.

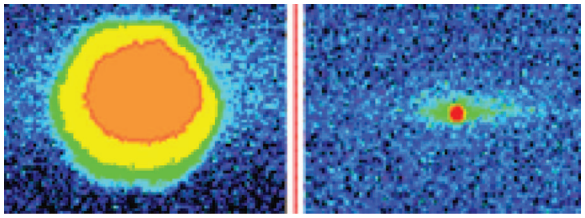

FIG. 5. False color image taken at 20 kV and 0.05 mA for 5 s at 20 mm (left) and 50 mm (right) from the lens output.

using Fuji HR-V computed radiography image plates with 50 μm pixel size. Images were taken at several distances from the lens, as shown in Fig. 5. A Gaussian fit to image profiles was used to estimate the spot size at each lens position. The FWHM for the images was plotted versus distance from the lens to find the location and size of focal spot.

The focal spot size was further quantified using a knife-edge scanning method. A sharp shielding knife edge was moved across the beam at the focal point. Measured counts were plotted against knife-edge position, showing a sigmoidal curve. The numerical derivative of the curve was fitted with a Gaussian to estimate the focal spot size.

The width of the focal spot arises from the divergence, α, from each individual capillary channel, as shown in Fig. 6. The focal spot size can be estimated as

$$s = d_{\text{out}} + 2f\alpha, \tag{2}$$

where d_{out} is the channel diameter of the capillary at the output end of the optic, as shown in Fig. 6, and α is the output divergence.

If there were no absorption, the x rays could reflect from the glass walls at angles up to the critical angle, so that $\alpha \sim \theta_c$, which is about 1.5 mrad at 20 keV. For real surfaces, the reflectivity is low near the critical angle θ_c, so fewer rays have reflected at an angle this high. The spot size was found to be consistent with a typical divergence of 1.3 θ_c.[17] This has been measured for several optics by measuring the width of the rocking curve of the diffraction from a nearly perfect crystal. The measured values of the beam spot and divergence were used in the simulation of the x-ray distribution.

Once the focal spot size was measured, PMMA blocks of varying thickness were placed between the optic and focal point to determine whether the focusing of the beam was maintained through the tissue.

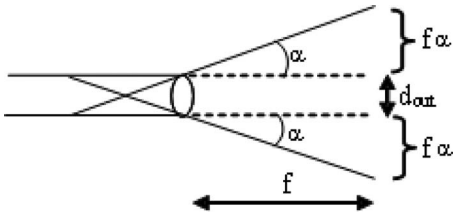

FIG. 6. Schematic for estimating spot size from the local divergence from a single capillary channel.

2.B. Simulating a focused x-ray beam using MCNP5

Monte Carlo simulations were used for dose calculation from a focused x-ray beam. MCNP5 was used to simulate a focused x-ray beam using measured beam parameters, including spectra and focal spot size. MCNP5 (Monte Carlo N-Particle Transport Code version 5) is a general purpose Monte Carlo code commonly used for simulating neutron, electron, photon, or coupled neutron/photon/electron transport through any media.[11] In MCNP5, source particles are defined using the source definition, "SDEF" card. Different types of source definitions are possible in MCNP5, including planar, point-isotropic, etc. Parameters on the SDEF card include starting position, source cell or surface, particle type, source energy, etc.[11] MCNP5 does not have a predefined source template for a focused beam, so instead an array of rays was generated to model the polycapillary optic. A C++ program was written to produce hundreds of positions (x, y, z) of source particles and the corresponding direction vectors (u, v, w) which were used in the SDEF card of MCNP5 to define a convergent beam. Starting positions of the source particles (x, y, z) were generated as random numbers inside a circular disk of radius 0.2 cm. The corresponding direction vectors (u, v, w) were defined such a way that the source particles passed through the focal point of the optic at 5 cm ($u = -x$, $v = -y$, $w = f$). Since, as noted, a polycapillary optic has some divergence and thus does not produce a perfect focus, a small random value was added to the direction of the source particles. The uniform distribution used slightly overestimates the effect of the finite source size compared to a more realistic Gaussian distribution. This may cause a slight underestimate of the dose concentration. The offset in the direction vectors was defined as

$$\theta = 1.3\theta_c\left(\text{rand}_1 - \frac{1}{2}\right), \tag{3}$$

where rand_1 is a uniform random number between 0 and 1. The azimuthal direction of the offset was given as

$$\varphi = (2\pi)\text{rand}_2, \tag{4}$$

where rand_2 was an independent uniform random number. The offsets in the direction vector thus became

$$\text{Offset}(u) = \sqrt{x^2 + y^2 + z^2}\,\sin(\theta)cos(\varphi), \tag{5}$$

$$\text{Offset}(v) = \sqrt{x^2 + y^2 + z^2}\,\sin(\theta)sin(\varphi). \tag{6}$$

Once the starting positions and the corresponding vectors with offsets were defined, they were then given to MCNP5 using the SDEF card.

Flux and dose distribution data were calculated using the MCNP5 superimposed mesh tally (fmesh4). The mesh tally divided the tissue phantom volume into a grid of orthogonal voxels and the x-ray flux in each voxel was calculated. Calculated flux in each voxel was converted to dose rate using a standard flux-to-dose table (ICRP-21) given in the MCNP5 manual.[11] The table was entered into the input file as a tally multiplier card. A tally multiplier card (FMn) is one of the optional features for tallies listed in MCNP5 manual.[11]

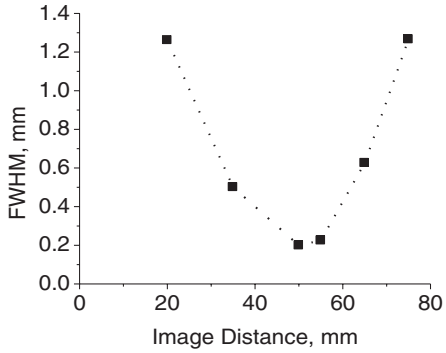

FIG. 7. Output focal spot width, taken at 20 kV and 0.05 mA, as a function of distance from the lens output. The focal spot size is 200 μm at a distance of 50 mm.

3. RESULTS

A Gaussian fit to image profiles was used to estimate the measured width at the focal point, as shown in Fig. 7.

The minimum width, measured with 50 μm pixels, was found to be 200 $\pm$ 50 μm at the output focal point distance of 50 mm with a 10 mm depth of field. In the MCNP5 simulation, after defining the focused beam, the focal spot size of the beam was verified by calculating the flux within a grid of voxels along the x axis at the focal plane, as shown in Fig. 8. The calculated width was 150 $\pm$ 90 μm, which was in good agreement with the measured spot size. The agreement shows the focus of the lens has been correctly modeled.

Once the focal spot size was measured, PMMA blocks of varying thickness were placed between the optic and focal point to determine whether the focusing of the beam was maintained through the tissue, as determined by knife-edge scans through the focal point. In order to understand the effects of photon energy on beam size, the measurements were performed with ~2 keV energy windows using the HpGE detector, as shown in Fig. 9. Both the incident and detected beams were broadband, and collected over a large energy range. The result shows that the focal point is well maintained up to 4 cm into the plastic. The spot size decreases with beam energy according to Eq. (2), because the critical angle, and hence the divergence α, decreases with photon energy. The slight decrease in spot size with depth is due to beam hardening effects, as a larger fraction of the transmitted photons will be at the high end of each given detector energy window after the beam passes through the plastic.

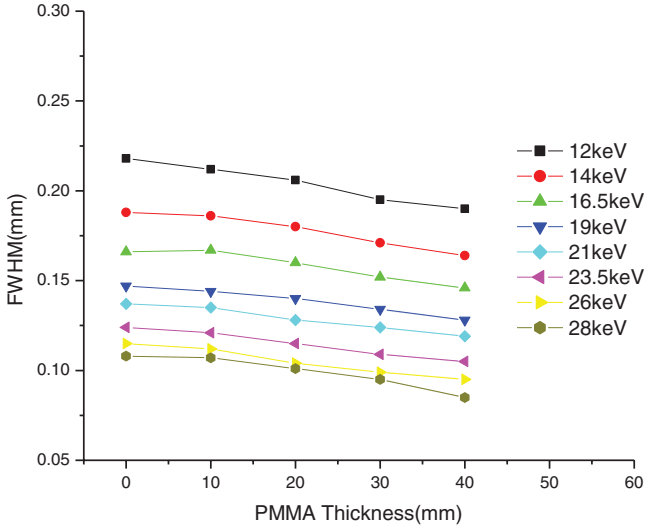

FIG. 9. Spot size versus phantom thickness.

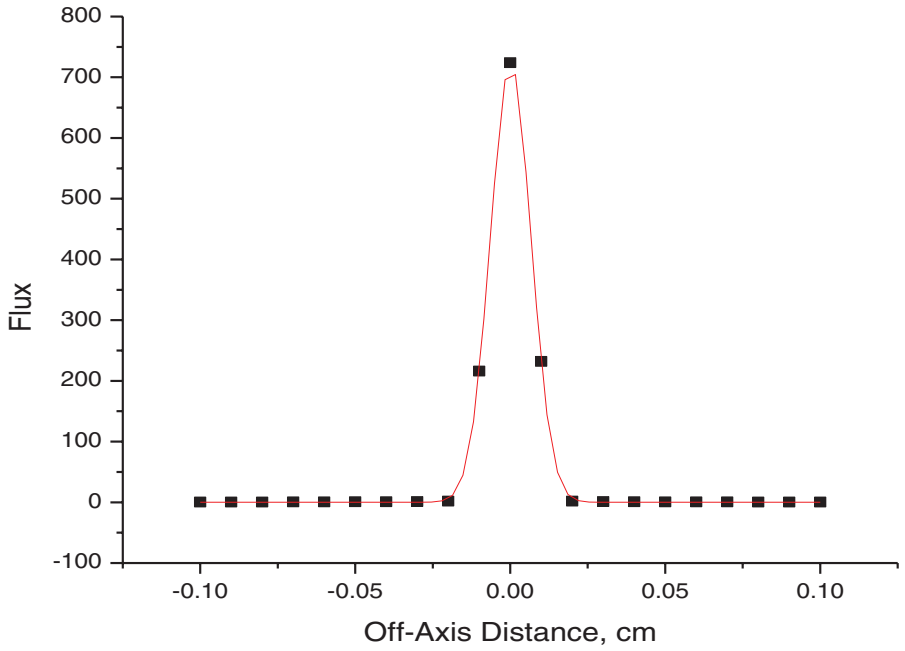

FIG. 8. Flux calculated across a grid of voxels on x axis at focal plane.

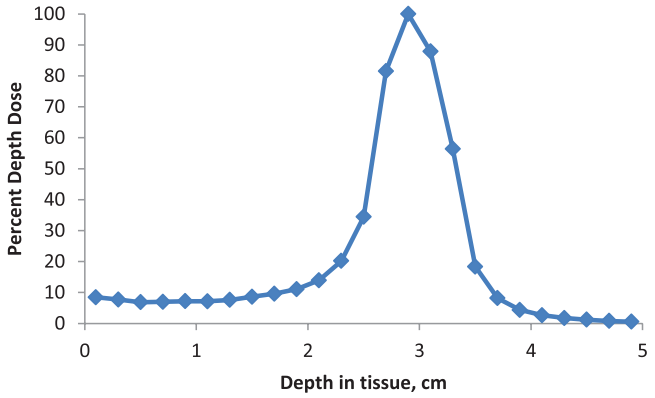

FIG. 10. Percent depth dose calculated by MCNP5 in tissue phantom for a single beam from a static optic.

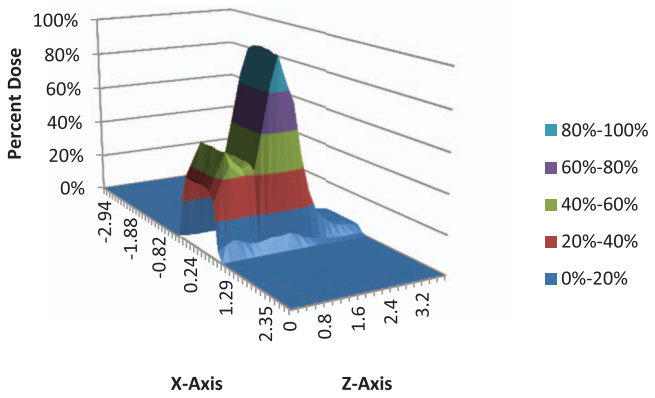

FIG. 11. Dose distribution calculated with superimposed mesh tally inside the patient geometry for a linear scan (tumor is from 1.4 to 2.4 cm along z axis). As expected, a simple linear scan would cause the near surface dose to rise. Beam rotation is required.

3.A. Static optic

Relative dose was calculated along the central axis of the beam from a static lens. A breast tissue phantom was simulated in shape of a hemisphere in MCNP5. The optic was positioned at 2 cm from the skin surface and the beam was focused at 3 cm inside the tissue. For dose calculations, cubic voxels of 0.2 mm side length were simulated along the central axis of the beam. The energy deposition in each voxel was calculated using the *F8 tally of MCNP5. Percent depth dose calculated inside the phantom is shown in Fig. 10. The focused beam was found to concentrate the dose within the tumor with sharp fall off before and after the treatment volume. Surface dose was below 10% for static optic.

3.B. Linear scan

Because the focal spot size of the beam is so small, a scan would be necessary to irradiate a reasonable size tumor. In a linear scan of the tumor, the x-ray beam would overlap due to the conical shape of the beam, so simply overlapping the lens position along a straight line will not be as skin sparing as desired. To demonstrate that, a single 0.02 cm thick slice of a 1 × 1 cm rectangular tumor was simulated in a cubical tissue with dimension 6 × 6 × 4 cm^3. The thickness of the tumor slice in y-direction was chosen equal to the focal spot size of the x ray beam (0.02 cm) and the height of the tumor was chosen equal to the field depth of the focused beam. The tissue surface was at 3.6 cm from the optic and the tumor was 1.4 cm deep in the tissue. In order to scan the tumor, the lens position was moved in the simulation using the "translation-rotation," "TR," option in the source definition, "SDEF," card. The TR option can be used to define source at several different positions.[11] The material for the tumor and the phantom was chosen as a soft tissue in the simulation. A linear scan was performed in the x-direction. The optic was translated in 50 steps to cover 1 cm along x axis. The dose distribution calculated with superimposed mesh tally is shown in Fig. 11. The skin dose was ~20% compared to peak dose in center of the tumor. A cross dose profile for the linear scan is shown in Fig. 12, which shows good uniformity, with rapid fall off of dose outside the tumor.

3.C. Rotation scan

As is well-known for megavoltage therapy, rotating the beam to expand the surface area provides a skin sparing effect. To demonstrate the advantages of rotation, a cylindrical tumor with a volume of 63 mm^3 was simulated in a spherical tissue of radius 3 cm. The optic was rotated in one plane around the sphere. The calculated dose distribution for a rotation scan is presented in Fig. 13. Skin dose was below 10% for the case in which it is possible to rotate the optic around the patient. Only a small volume was treated. A larger tumor would require scanning in the out of plane dimension.

3.D. Scan and rotate

To accommodate a larger tumor without creating repeated overlap at the skin surface, the beam could be rotated while it is scanned. Rotating the beam as it is scanned would maintain the beam spreading and preserve the skin sparing effect. The focused beam was rotated by a small angle with each translation to cover a single 0.02 cm slice of a rectangular 1 × 1 cm tumor, again in a cubical tissue with rectangular dimension 6 × 6 × 4 cm^3. The optic was translated and rotated at 50 different positions to cover the tumor. This was accomplished

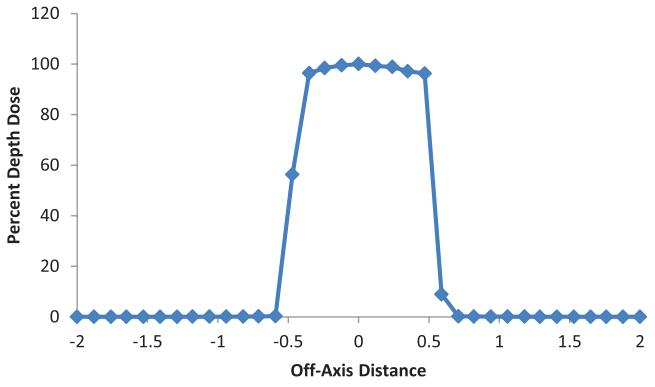

FIG. 12. Cross dose profile calculated at center of tumor for the linear scan.

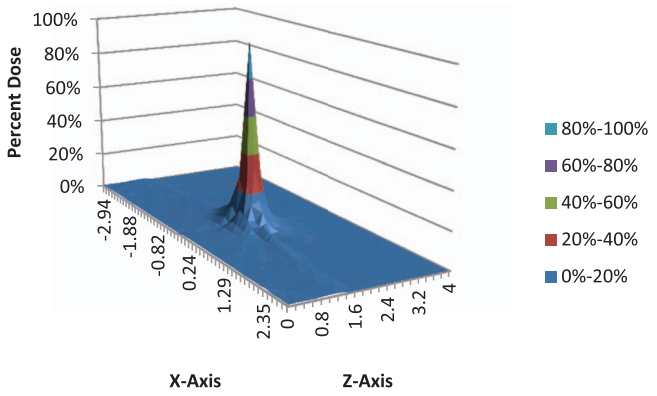

FIG. 13. Dose distribution calculated with superimposed mesh tally for a cylindrical tumor at the focal point of the beams which were rotated about the tumor axis (tumor is from 1.4 to 2.4 cm along z axis).

by changing the source location for the jth step as

$$\begin{aligned} x'_j &= x + f\sin(j\Delta\theta) + \Delta x, \\ z'_j &= z + f(1-\cos(j\Delta\theta)), \\ \theta_{x,x'} &= j\Delta\theta, \\ \theta_{z,x'} &= 90^\circ - j\Delta\theta, \\ \theta_{x,z'} &= 90^\circ + j\Delta\theta, \\ \theta_{x,y'} &= \theta_{z,y'} = \theta_{y,x'} = \theta_{y,z'} = 90^\circ, \\ \theta_{z,z'} &= \theta_{y,y'} = 0, \end{aligned} \tag{7}$$

where the primed coordinates are the axes after rotation and translation, f is the focal distance of the lens, and, as required by the MCNP TR card, the angles are stated between each pair of primed and unprimed coordinate axes. The step sizes were $\Delta x = 2$ mm for translation and $\Delta\theta = 2^\circ$ for rotation. The dose distribution calculated with the superimposed mesh tally is shown in Fig. 14. The skin sparing effects of the focused beam were preserved when the beam was angled as it was translated. The peak to skin dose ratio was 45. To cover a large tumor, rotation about the orthogonal (x) axis would be used as the beam is stepped in y. This would preserve a sharp dose peak in the desired volume with a low skin dose.

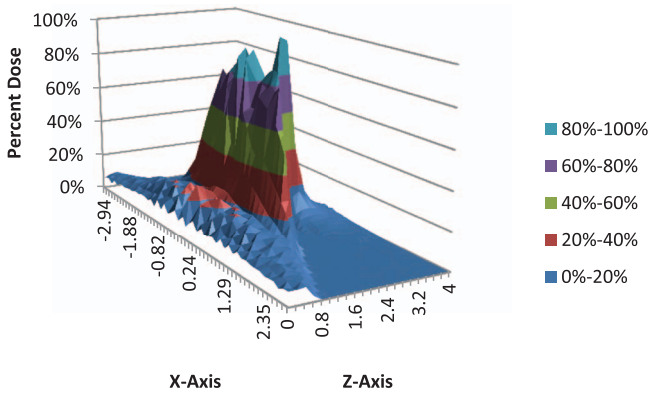

FIG. 14. Dose distribution inside the patient geometry for a translated and rotated beam (tumor is from 1.4 to 2.4 cm along z axis).

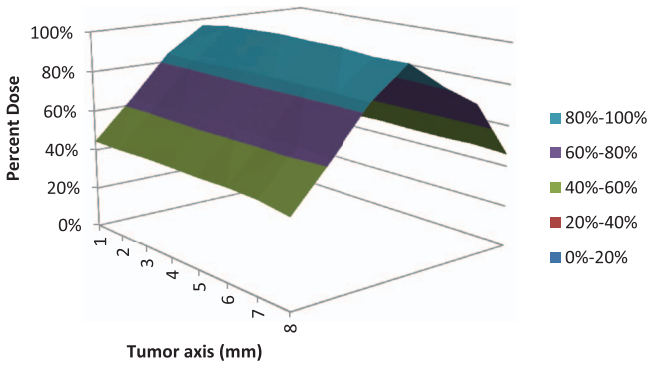

FIG. 15. Dose heterogeneity inside the tumor for the translate and rotate scan.

Dose heterogeneity inside tumor is shown in Fig. 15 for the scan and rotate method. Because the scan was stopped at the edges of the tumor, there was a drop off in dose at the edges. Sixty percent of the tumor received 87% of prescribed dose and minimum tumor dose was around 40% of the prescribed dose. Although proposed method produced high heterogeneous dose distribution, a more homogenous dose distribution would be achieved by employing both a wider scan and by breaking the scan into a larger number of source steps.

The proposed method has potential for better skin sparing compared to the megavoltage photon beams in treating the soft tissue. Estimates from the measured beam transmissions on the plastic phantom could be performed by scaling up from the 2.5 W source to a 50 kW source more appropriate for rapid irradiation. In that case, the estimates indicated that a scan to cover a 1 cm^3 tumor with a dose of 2 Gy could be performed in a few minutes.[16] This is consistent with the MCNP calculations, which gave a dose of 1.1 cGy per 60×10^6 photons for the $0.02 \times 0.02 \times 0.2$ cm^3 voxel at the focal point. Since the lens transmitted 3.6×10^{10} photons/s A of source current, a 50 kW source would yield a dose of 2 Gy to the focal voxel in 0.36 s. The depth of field of the optic is about 1 cm, so it is only necessary to scan in 2D to cover a 1 cm^3 tumor. Doing this in 0.02 cm steps would require less than 15 min.

4. CONCLUSION

A focused x-ray beam was obtained with polycapillary optics. The focusing was maintained in 40 mm of PMMA phantom. Measured parameters were used to simulate a focused x-ray beam in MCNP5. Skin sparing is important in radiation therapy and is the limiting factor in dose escalation. Dose simulations gave high conformal dose to the tumor while sparing the skin was achieved by scanning the tumor while rotating the polycapillary optic. Low energy focused x-ray beams could be used to irradiate the tumors inside soft tissue within 5 cm of the surface with the potential for better skin sparring compared to the megavoltage photon beams.

ACKNOWLEDGMENTS

The authors wish to acknowledge discussion with the late Professor Walter Gibson, and support from NIH # 7 R01 EB009715.

[a]Author to whom correspondence should be addressed. Electronic mail: Hassan.Abbas@Yale.Edu; Telephone: 518-894-7549; Fax: (203) 688-8682.
[b]Electronic mail: dip.n.mahato@intel.com.
[c]Electronic mail: sattij@mail.amc.edu.
[d]Electronic mail: c.macdonald@albany.edu.

[1]V. A. Arkad'ev *et al.*, "Wide-band X-ray optics with a large angular aperture," Sov. Phys. Usp. **32**(3), 271–276 (1989).
[2]C. A. MacDonald and W. M. Gibson, "Polycapillary optics," in *Handbook of Optics: Atmospheric Optics, Modulators, Fiber Optics, X-Ray and Neutron Optics*, 3rd ed., edited by M. Bass, C. DeCusatis, J. Enoch, V. Lakshminarayanan, G. Li, C. A. MacDonald, V. N. Mahajan, and E. Van Stryland (McGraw-Hill, New York, 2010), Vol. V.
[3]W. Zhou, D. Mahato, and C. A. MacDonald, "Analysis of powder x-ray diffraction resolution using collimating and focusing polycapillary optics," Thin Solid Films **518**(18), 5047–5056 (2010).
[4]F. A. Hofmann, W. M. Gibson, C. A. MacDonald, D. A. Carter, J. X. Ho, and J. R. Ruble, "Polycapillary optic—Source combinations for protein crystallography," J. Appl. Cryst. **34**(3), 330–335 (2001).
[5]C. A. MacDonald and W. M. Gibson, "Applications and advances in polycapillary optics," X-ray Spectrom. **32**(3), 258–268 (2003).
[6]R. Fahrig, J. G. Mainprize, N. Robert, A. Rogers, and M. J. Yaffe, "Performance of glass fiber antiscatter devices at mammographic energies," Med. Phys. **21**(8), 1277–1282 (1994).
[7]N. Mail, C. MacDonald, and W. M. Gibson, "Microscintigraphy with high resolution collimators and radiographic imaging detectors," Med. Phys. **36**(2), 645–655 (2009).
[8]F. R. Sugiro, D. Li, and C. A. MacDonald, "Beam collimation with polycapillary X-ray optics for high contrast high resolution monochromatic imaging," Med. Phys. **31**(12), 3288–3297 (2004).
[9]C. C. Abreu and C. A. MacDonald, "Beam collimation, focusing, filtering and imaging with polycapillary X-ray and neutron optics," Phys. Med. **13**(3), 79–89 (1997).
[10]B. K. Rath, W. M. Gibson, Lei Wang, B. E. Homan, and C. A. MacDonald, "Measurement and analysis of radiation effects in polycapillary X-ray optics," J. Appl. Phys. **83**(12), 7424–7435 (1998).
[11]X-5 Monte Carlo Team, "MCNP5—A general N-particle transport code, Version 5," LA-CP-03-0245, April 2003.
[12]D. E. Wazer, L. Berle, R. Graham, M. Chung, J. Rothschild, T. Graves, B. Cady, K. Ulin, R. Ruthazer, and T. A. DiPetrillo, "Preliminary results of a phase I/II study of HDR brachytherapy alone for T1/T2 breast cancer," Int. J. Radiat. Oncol., Biol., Phys. **53**(4), 889–897 (2002).
[13]N. M. Shah, T. Tenenholz, D. Arthur, T. DiPetrillo, B. Bornstein, G. Cardarelli, Z. Zheng, M. J. Rivard, S. Kaufman, and D. E. Wazer, "MammoSite and interstitial brachytherapy for accelerated partial breast irradiation: Factors affecting toxicity and cosmesis," Cancer **101**(4), 727–734 (2004).
[14]A. Dickler and K. Dowlatshahi, "Xoft Axxent electronic brachytherapy," Expert Rev. Med. Dev. **6**(1), 27–31 (2009).
[15]G. Jost *et al.*, "Photelectric-enhanced radiation therapy with quasimonochromatic computed tomography," Med. Phys. **36**(6), 2107–2117 (2009).
[16]D. N. Mahato and C. A. MacDonald, "Potential for focused beam orthovoltage therapy," Proc. SPIE **7806**, 78060F (2010).
[17]C. A. MacDonald, "Focusing polycapillary optics and their applications," X-Ray Opt. Instrum. **2010**, 867049.